

Role of a finite exposure time on measuring an elastic modulus using microrheology

Thierry Savin and Patrick S. Doyle*

*Chemical Engineering Department, Massachusetts Institute of Technology, 77 Massachusetts Avenue,
Cambridge, Massachusetts 02139, USA*

(Received 24 November 2004; published 25 April 2005)

The role of a finite exposure time σ on measuring rheological properties using microrheology techniques is theoretically investigated. We concentrate on studying fluid models displaying a plateau in the mean-squared displacement (MSD) of the embedded probe particle. A model is developed to compare the resulting experimentally measured MSD of the particle to its expected value in the fluid model. A plateau MSD is greatly modified in a measurement when σ is greater than the plateau onset time. Moreover, apparent dynamics drastically differ from the true dynamics at frequencies $\omega \lesssim \sigma^{-1}$. These results quantify when and how a finite exposure time effects the measured MSD of a probe particle which can then alter the extracted rheological properties and physical interpretations.

DOI: 10.1103/PhysRevE.71.041106

PACS number(s): 05.40.-a, 83.10.Pp, 83.60.-a, 83.85.Cg

I. INTRODUCTION

Passive microrheology uses thermally fluctuating micron-sized probes to determine local mechanical properties of a host medium [1]. In this class of techniques, time correlation of the particle position or displacement, through either the power spectral density $S_{\mathbf{x}}^*(\omega) = \langle |\mathbf{x}^*|^2(\omega) \rangle$ or the mean-squared displacement $\langle \Delta \mathbf{x}^2(t) \rangle = \langle [\mathbf{x}(\theta+t) - \mathbf{x}(\theta)]^2 \rangle$, is often calculated [2,3]. Here $\mathbf{x}(t)$ is the particle position at time t , $\mathbf{x}^*(\omega)$ is its Fourier transform at the frequency ω , and the brackets $\langle \dots \rangle$ indicate an ensemble average over a particle population and/or a time average over θ . Using a generalized Stokes expression for the drag applied on the particle by the medium (continuum assumption) and the fluctuation-dissipation theorem (thermal equilibrium assumption), these correlations can then be related to the shear modulus spectrum $G^*(\omega)$ of the material over a large frequency range [2,4]. This range is limited in the high frequencies by the fluid and/or the probe inertial effects (1–10 MHz in usual conditions), and in the low frequencies by the network compressibility (less than 1 Hz) [2,5,6]. The Brownian motion of a particle embedded in a complex fluid thus involves time scales from a variety of dynamical regimes, including the material viscoelastic relaxation modes.

Several techniques can be used to measure the particles position correlations (see Ref. [7] for a review). Recently, we outlined a general classification of the errors arising in these techniques [8]. On the one hand, the noise in the detection scheme induces an error independent of the particle dynamics, and thus can be measured with a static particle and corrected on the averaged time correlations. On the other hand, the sampling method of the particle motions leads to an error that depends on the particle dynamics, and is challenging to correct. The latter error is referred to as “dynamic error” in the following study.

This work focuses on the role of a finite exposure time and the resulting dynamic-dependent errors when measuring

an elastic modulus using microrheology techniques. The first section shows the general expression for the apparent mean-squared displacement resulting from the propagation of these errors on the true mean-squared displacement. The second part explores three model fluids exhibiting a purely elastic regime, for which the dynamic error can have a dramatic effect. In the third section, we discuss implications of these results on microrheology measurements.

II. DYNAMIC ERROR

Experimentally, microrheology involves measuring particle displacements using some sort of detector (e.g., CCD for video microscopy or quadrant photodiode for laser deflection tracking). A single measurement requires a given exposure time σ during which the particle is continually moving. Thus, the position that is acquired at time t contains the history of the successive positions occupied by the particle during the time interval $[t-\sigma, t]$. We model this dynamic error by calculating the measured position as the average $\bar{\mathbf{x}}(t, \sigma)$ of all the positions the particle takes during the acquisition [9],

$$\bar{\mathbf{x}}(t, \sigma) = \frac{1}{\sigma} \int_0^\sigma \mathbf{x}(t - \xi) d\xi. \quad (1)$$

The finite sampling acts as a moving average low-pass linear filter [10]. To estimate $\langle \Delta \bar{\mathbf{x}}^2(t, \sigma) \rangle$, we use a method similar to that used in Ref. [11] and we write

$$\bar{\mathbf{x}}(\theta + t, \sigma) - \bar{\mathbf{x}}(\theta, \sigma) = \frac{1}{\sigma} \int_0^\sigma d\xi' \int_\theta^{\theta+t} dt' \mathbf{v}(t' - \xi'), \quad (2)$$

where $\mathbf{v}(t)$ is the true velocity of the particle. In terms of the velocity autocorrelation function $C_{\mathbf{v}}(|t'' - t'|) = \langle \mathbf{v}(t') \cdot \mathbf{v}(t'') \rangle$, we find

*Author to whom correspondence should be addressed. Email address: pdoyle@mit.edu

$$\begin{aligned}
\langle \Delta \bar{\mathbf{x}}^2(t, \sigma) \rangle &= \langle [\bar{\mathbf{x}}(\theta + t, \sigma) - \bar{\mathbf{x}}(\theta, \sigma)]^2 \rangle \\
&= \frac{1}{\sigma^2} \int_0^\sigma d\xi' \int_0^\sigma d\xi'' \int_0^t dt' \int_0^t dt'' \\
&\quad \times C_v(|(t' - \xi') - (t'' - \xi'')|) \\
&= \frac{2}{\sigma^2} \int_0^\sigma d\xi (\sigma - \xi) \int_0^t d\theta (t - \theta) \\
&\quad \times [C_v(\theta + \xi) + C_v(|\theta - \xi|)]
\end{aligned}$$

after multiple changes of variable and partial integrations. By comparing this expression to the similar expression obtained for the true mean-squared displacement [11],

$$\langle \Delta \mathbf{x}^2(t) \rangle = 2 \int_0^t (t - \theta) C_v(\theta) d\theta, \quad (3)$$

we finally find, under the condition $t \geq \sigma$,

$$\begin{aligned}
\langle \Delta \bar{\mathbf{x}}^2(t, \sigma) \rangle &= \frac{1}{\sigma^2} \int_0^\sigma [\langle \Delta \mathbf{x}^2(t + \xi) \rangle + \langle \Delta \mathbf{x}^2(t - \xi) \rangle - 2\langle \Delta \mathbf{x}^2(\xi) \rangle] \\
&\quad \times (\sigma - \xi) d\xi. \quad (4)
\end{aligned}$$

This relation is linear, but in general is difficult to invert.

We present in the next section three relevant examples for model viscoelastic fluids in which Brownian particles exhibit a known mean-squared displacement $\langle \Delta \mathbf{x}^2(t) \rangle$. These examples give specific insight into how the resulting measured mean-squared displacement $\langle \Delta \bar{\mathbf{x}}^2(t, \sigma) \rangle$ compares with the true mean-squared displacement $\langle \Delta \mathbf{x}^2(t) \rangle$.

III. FLUID MODELS

A. Power-law relaxation model

We first consider a toy-model where the mean-squared displacement has the following form:

$$\frac{\langle \Delta \mathbf{x}^2(t) \rangle}{\langle \Delta \mathbf{x}_p^2 \rangle} = \begin{cases} (t/\tau)^\alpha & \text{if } t \leq \tau, \\ 1 & \text{if } t > \tau, \end{cases} \quad (5)$$

where $\langle \Delta \mathbf{x}_p^2 \rangle$ is the plateau value and τ is the characteristic time required to reach this plateau. The fluctuation-dissipation theorem and the generalized Stokes relation gives $\langle \Delta \mathbf{x}_p^2 \rangle = k_B T / (\pi a G)$, where a is the radius of the spherical particle, G is the elastic modulus of the medium, and $k_B T$ is the Boltzmann temperature. The mean-squared displacement described by this model is qualitatively observed in many systems, though the sharp break introduced at $t = \tau$ is not physically realistic. This model allows us to consider on one hand the characteristic plateau onset time τ , as well as the nature of the particle dynamics through the exponent α .

For this model, we find that a plateau is reached for $t > \bar{\tau}(\sigma)$, where $\bar{\tau}(\sigma) = \tau + \sigma$ is the apparent relaxation time, and takes the following values:

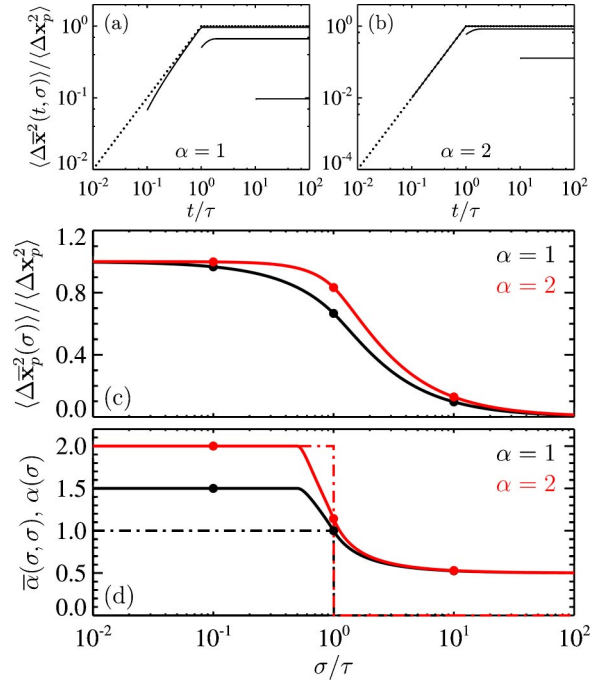


FIG. 1. (Color online) Results for the power-law relaxation model. (a) and (b) are the exact mean-squared displacement (dotted lines) from Eq. (5) and its apparent values (solid lines) obtained from Eq. (4) with $\sigma/\tau = 0.1, 1$, and 10 . (c) shows the apparent plateau values, as given by Eq. (6). The filled circles correspond to the three values of σ/τ used in (a) and (b). (d) is the short-time power-law scaling [Eq. (7), solid lines] vs σ/τ . The dashed-dotted lines are the values for the exact scaling $\alpha(t = \sigma)$.

$$\frac{\langle \Delta \bar{\mathbf{x}}_p^2(\sigma) \rangle}{\langle \Delta \mathbf{x}_p^2 \rangle} = \begin{cases} 1 - \frac{2(\sigma/\tau)^\alpha}{(1 + \alpha)(2 + \alpha)} & \text{if } \sigma \leq \tau, \\ \frac{\alpha}{(\sigma/\tau)^2} \left(\frac{2(\sigma/\tau)}{1 + \alpha} - \frac{1}{2 + \alpha} \right) & \text{if } \sigma > \tau. \end{cases} \quad (6)$$

One can also calculate the apparent short-time power law $\bar{\alpha}(t = \sigma, \sigma)$ where the local apparent power-law scaling is defined by

$$\bar{\alpha}(t, \sigma) = \frac{d(\log \langle \Delta \bar{\mathbf{x}}^2(t, \sigma) \rangle)}{d(\log t)}. \quad (7)$$

We show in Fig. 1 the evolution of these quantities as a function of the acquisition time σ . Effects of the finite sampling become important for $\sigma \geq \tau$. The apparent plateau value vanishes when $\sigma \gg \tau$ as shown in Fig. 1(a). More dramatic is the effect of the sampling process on the short-time power-law scaling [Fig. 1(d)]. In general, the true scaling is not recovered in the apparent mean-squared displacement when $\sigma \leq t \leq \tau$ [16]. An exception to this is the ballistic case $\alpha = 2$ for which measured displacements are independent of σ , as shown by plugging a constant velocity $\mathbf{v}(t) = \mathbf{v}$ in Eq. (2).

B. Voigt fluid model

The shear modulus spectrum of the Voigt fluid viscoelastic model is given by

$$G^*(\omega) = G(1 + i\omega\tau_v), \quad (8)$$

where G is the elastic modulus and τ_v is the relaxation time. The equation governing the particle dynamics for this model is then given by

$$\tau_v \tau_b \ddot{\mathbf{x}}(t) + \tau_v \dot{\mathbf{x}}(t) + \mathbf{x}(t) = \mathbf{f}(t)/(6\pi a G), \quad (9)$$

where $\tau_b = m/(6\pi a G \tau_v)$ is the Brownian time (m being the mass of the particle), and $\mathbf{f}(t)$ is the Brownian force [12]. By taking the Fourier transform on both sides of Eq. (9), we can calculate the power spectral density of the position by

$$S_{\mathbf{x}}^*(\omega) = \langle |\mathbf{x}^*|^2(\omega) \rangle = \frac{\tau_v k_B T / (\pi a G)}{(1 + \tau_+^2 \omega^2)(1 + \tau_-^2 \omega^2)}, \quad (10)$$

where we have introduced the relaxation times

$$\tau_{\pm} = \frac{\tau_v}{2} (1 \pm \sqrt{1 - 4\tau_b/\tau_v}), \quad (11)$$

that can be complex numbers in the underdamped case $4\tau_b > \tau_v$. To write Eq. (10), we have also used the fluctuation-dissipation theorem $S_{\mathbf{f}}^*(\omega) = \langle |\mathbf{f}^*|^2(\omega) \rangle = 36\pi a G \tau_v k_B T$. The inverse Fourier transform of $S_{\mathbf{x}}^*(\omega)$ gives the position autocorrelation function $C_{\mathbf{x}}(t)$ and we use the relation $\langle \Delta \mathbf{x}^2(t) \rangle = 2C_{\mathbf{x}}(0) - 2C_{\mathbf{x}}(t)$ to find

$$\frac{\langle \Delta \mathbf{x}^2(t) \rangle}{\langle \Delta \mathbf{x}_p^2 \rangle} = \frac{\tau_+ (1 - e^{-|t|/\tau_+}) - \tau_- (1 - e^{-|t|/\tau_-})}{\tau_+ - \tau_-}. \quad (12)$$

For the overdamped regime $4\tau_b/\tau_v \ll 1$, shown in Fig. 2(a), a plateau region is obtained for $t \gg \tau_v$. However, for the underdamped limit $4\tau_b/\tau_v \gg 1$, plotted in Fig. 2(b), the plateau is reached for $t \gg \sqrt{\tau_b \tau_v}$ and the mean-squared displacement exhibits oscillations around the plateau value with a period of $\sim 2\pi\sqrt{\tau_b \tau_v}$.

Using Eq. (4), we can calculate the apparent mean-squared displacement $\langle \Delta \bar{\mathbf{x}}^2(t, \sigma) \rangle$ and obtain the plateau value by letting $t \gg \max(\tau_v, \sqrt{\tau_b \tau_v})$,

$$\frac{\langle \Delta \bar{\mathbf{x}}_p^2(\sigma) \rangle}{\langle \Delta \mathbf{x}_p^2 \rangle} = \frac{\tau_+ + \tau_-}{\sigma/2} - \frac{\tau_+^3 (1 - e^{-\sigma/\tau_+}) - \tau_-^3 (1 - e^{-\sigma/\tau_-})}{\sigma^2 (\tau_+ - \tau_-)/2}. \quad (13)$$

We first consider the overdamped limit. In that case, the characteristic timescale is τ_v and Eq. (13) simplifies to

$$\frac{\langle \Delta \bar{\mathbf{x}}_p^2(\sigma) \rangle}{\langle \Delta \mathbf{x}_p^2 \rangle} = \frac{\tau_v}{\sigma/2} - \frac{1 - e^{-\sigma/\tau_v}}{(\sigma/\tau_v)^2/2} + O(\tau_b/\tau_v) \quad (14)$$

as obtained by keeping σ/τ_v finite and $\tau_b/\tau_v \rightarrow 0$.

It is interesting to consider the underdamped regime of the Voigt model since we will show it is similar to the short-time behavior of the Maxwell model in the next section. The apparent plateau value is obtained by keeping $\sigma/\sqrt{\tau_b \tau_v}$ finite and $\tau_v/\tau_b \rightarrow 0$,

$$\frac{\langle \Delta \bar{\mathbf{x}}_p^2(\sigma) \rangle}{\langle \Delta \mathbf{x}_p^2 \rangle} = \text{sinc}^2\left(\frac{\sigma}{2\sqrt{\tau_b \tau_v}}\right) + O((\tau_v/\tau_b)^{1/2}), \quad (15)$$

where $\text{sinc}(x) = \sin(x)/x$ is the sine cardinal function. Note that the same results would have been obtained if the follow-

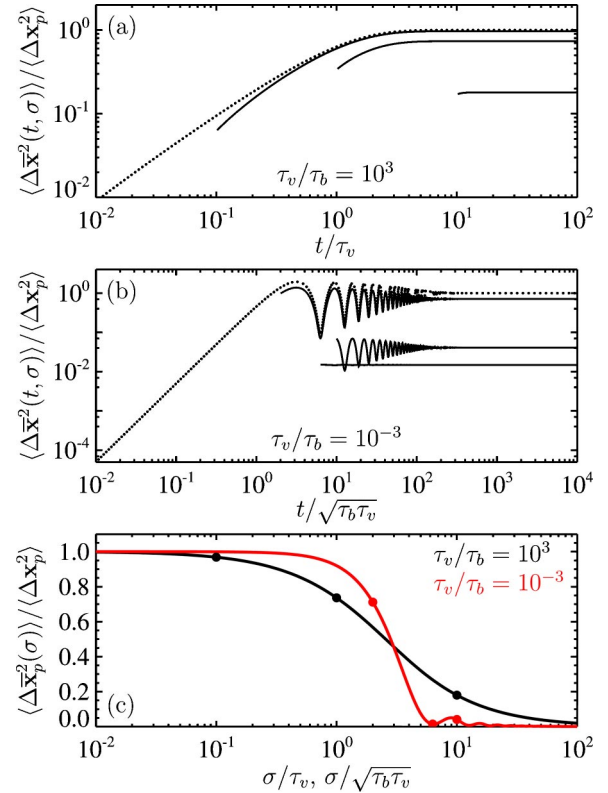


FIG. 2. (Color online) Results for the Voigt fluid model. (a) and (b) are the exact mean-squared displacement (dotted lines) from Eq. (12) and its apparent value (solid lines) obtained from Eq. (4) with $\sigma/\tau_v = 0.1, 1, 10$ in (a), and $\sigma/\sqrt{\tau_b \tau_v} = 2, 2\pi, 10$ in (b). (c) shows the apparent plateau values, as given by Eq. (13). The filled circles on each line denote the values of σ used in (a) and (b).

ing approximated mean-squared displacement were plugged into Eq. (4):

$$\frac{\langle \Delta \mathbf{x}^2(t) \rangle}{\langle \Delta \mathbf{x}_p^2 \rangle} = \begin{cases} 1 - e^{-t/\tau_v} + O(\tau_b/\tau_v), \\ 1 - \cos(t/\sqrt{\tau_b \tau_v}) + O((\tau_v/\tau_b)^{1/2}), \end{cases} \quad (16)$$

by, respectively, keeping t/τ_v or $t/\sqrt{\tau_b \tau_v}$ finite. In particular, the apparent mean-squared displacement in the inertialess limit $\tau_b/\tau_v = 0$ is found to be [8]

$$\frac{\langle \Delta \bar{\mathbf{x}}^2(t, \sigma) \rangle}{\langle \Delta \mathbf{x}_p^2 \rangle} = \epsilon_\sigma (1 - \beta_\sigma e^{-t/\tau_v}), \quad (17)$$

with

$$\epsilon_\sigma = \frac{\langle \Delta \bar{\mathbf{x}}_p^2(\sigma) \rangle}{\langle \Delta \mathbf{x}_p^2 \rangle} = \frac{\tau_v}{\sigma/2} - \frac{1 - e^{-\sigma/\tau_v}}{(\sigma/\tau_v)^2/2}, \quad (18)$$

$$\beta_\sigma = 1 - \frac{\sinh(\sigma/\tau_v) - \sigma/\tau_v}{1 - e^{-\sigma/\tau_v} - \sigma/\tau_v}. \quad (19)$$

Similar to the power-law relaxation model, the plateau value shown in Fig. 2(c) is greatly modified by the finite sampling for σ greater than the characteristic plateau onset time. In the underdamped case, the plateau is reached

through oscillations and its apparent value is nonmonotonically decreasing with increasing acquisition time [cf. the oscillating line in Fig. 2(c)].

C. Maxwell fluid model

In the single relaxation time Maxwell fluid viscoelastic model, the shear modulus spectrum is given by

$$G^*(\omega) = G \frac{i\omega\tau_m}{1 + i\omega\tau_m}, \quad (20)$$

where G is the elastic modulus and τ_m is the relaxation time. The equation governing the particle dynamics for this model is then

$$\tau_m \tau_b \ddot{\mathbf{v}}(t) + \tau_b \dot{\mathbf{v}}(t) + \mathbf{v}(t) = \mathbf{f}(t) / (6\pi a G \tau_m), \quad (21)$$

where $\mathbf{v}(t) = \dot{\mathbf{x}}(t)$ is the velocity of the particle [12]. By taking the Fourier transform on both sides of Eq. (21), we can calculate the power spectral density of the velocity by

$$S_v^*(\omega) = \langle |\mathbf{v}|^2(\omega) \rangle = \frac{k_B T / (\pi a G \tau_m)}{(1 + \tau_+^2 \omega^2)(1 + \tau_-^2 \omega^2)}, \quad (22)$$

where we have introduced the complex relaxation time

$$\tau_{\pm} = \frac{\tau_b}{2} (1 \pm i\sqrt{4\tau_m/\tau_b - 1}) \quad (23)$$

and we have used the fluctuation-dissipation theorem $S_f^*(\omega) = 36\pi a G \tau_m k_B T$. The inverse Fourier transform of $S_v^*(\omega)$ returns the velocity autocorrelation function $C_v(t)$ and the use of Eq. (3) gives finally [17]

$$\frac{\langle \Delta \mathbf{x}_p^2(t) \rangle}{\langle \Delta \mathbf{x}_p^2 \rangle} = \frac{|t|}{\tau_+} + \frac{|t|}{\tau_-} - \frac{\tau_+^3(1 - e^{-|t|/\tau_+}) - \tau_-^3(1 - e^{-|t|/\tau_-})}{\tau_+ \tau_- (\tau_+ - \tau_-)}. \quad (24)$$

We investigate only the physically realistic regime where $\tau_m/\tau_b \gg 1$.

For the Maxwell model, a plateau region is obtained for $\sqrt{\tau_b \tau_m} < t < \tau_m$ and its apparent value is found to be

$$\begin{aligned} \frac{\langle \Delta \bar{\mathbf{x}}_p^2(\sigma) \rangle}{\langle \Delta \mathbf{x}_p^2 \rangle} &= \lim_{t/\sqrt{\tau_b \tau_m} \rightarrow \infty} \left[\frac{\langle \Delta \bar{\mathbf{x}}^2(t, \sigma) \rangle}{\langle \Delta \mathbf{x}_p^2 \rangle} - \frac{t}{\tau_+} - \frac{t}{\tau_-} \right] \\ &= \frac{\tau_+^5(1 - e^{-\sigma/\tau_+}) - \tau_-^5(1 - e^{-\sigma/\tau_-})}{\sigma^2 \tau_+ \tau_- (\tau_+ - \tau_-)/2} - \frac{\tau_+ + \tau_-}{\sigma/2} \\ &\quad - \frac{\tau_+^3 + \tau_-^3}{\sigma \tau_+ \tau_- / 2} - \frac{\sigma}{3\tau_+} - \frac{\sigma}{3\tau_-}. \end{aligned} \quad (25)$$

For $2\pi\sqrt{\tau_b \tau_m} < \sigma \leq t$, the sampling rate is not high enough to detect the oscillations in the mean-squared displacement, and we introduce the following approximation [18]:

$$\frac{\langle \Delta \bar{\mathbf{x}}^2(t, \sigma) \rangle}{\langle \Delta \mathbf{x}_p^2 \rangle} \simeq \epsilon_\sigma \left(\frac{t}{\tau_m \epsilon_\sigma} + 1 \right), \quad (26)$$

with $\epsilon_\sigma = \langle \Delta \bar{\mathbf{x}}_p^2(\sigma) \rangle / \langle \Delta \mathbf{x}_p^2 \rangle$ and obtained by discarding oscillatory terms in $\langle \Delta \bar{\mathbf{x}}^2(t, \sigma) \rangle$. Equation (26) also shows that the apparent Maxwell relaxation time is

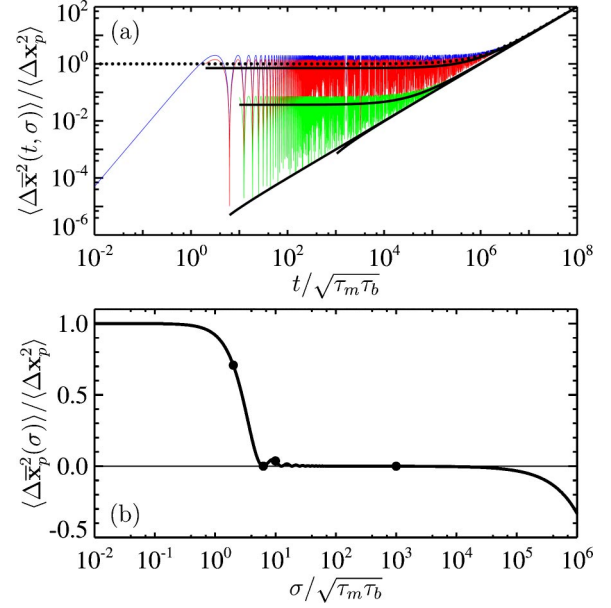


FIG. 3. (Color online) Results for the Maxwell fluid model, with $\tau_m/\tau_b = 10^{12}$ (motivation for this value is given in the Discussion section). (a) gives the true mean-squared displacement (dotted line) and its apparent value (solid lines) for $\sigma/\sqrt{\tau_b \tau_m} = 2, 2\pi, 10$, and 10^3 . The dotted and thick lines are obtained with Eq. (26) whereas the thin curves result from exact calculations using Eqs. (4) and (24). (b) shows the apparent plateau values as given by Eq. (25). The filled circles denote the values of σ used in (a).

$$\bar{\tau}_m(\sigma) = \tau_m \epsilon_\sigma. \quad (27)$$

Next, we calculate the limiting behavior of Eq. (25) as $\tau_b/\tau_m \rightarrow 0$. By keeping $\sigma/\sqrt{\tau_b \tau_m}$ finite, we obtain

$$\frac{\langle \Delta \bar{\mathbf{x}}_p^2(\sigma) \rangle}{\langle \Delta \mathbf{x}_p^2 \rangle} = \text{sinc}^2\left(\frac{\sigma}{2\sqrt{\tau_b \tau_m}}\right) + O((\tau_b/\tau_m)^{1/2}), \quad (28)$$

whereas by keeping σ/τ_m finite, we find

$$\frac{\langle \Delta \bar{\mathbf{x}}_p^2(\sigma) \rangle}{\langle \Delta \mathbf{x}_p^2 \rangle} = -\frac{\sigma}{3\tau_m} + O(\tau_b/\tau_m). \quad (29)$$

It is interesting to note the close resemblance of Eq. (15) to Eq. (28). This point will be discussed in the next section.

The inertialess regime is a peculiar limit where

$$\langle \Delta \bar{\mathbf{x}}^2(t, \sigma) \rangle = \frac{\langle \Delta \mathbf{x}_p^2 \rangle}{\tau_m} (t - \sigma/3) \quad (30)$$

is similar to the purely viscous model, for which $\langle \Delta \bar{\mathbf{x}}^2(t, \sigma) \rangle = 6D(t - \sigma/3)$, where D is the self-diffusion coefficient of the particle [8]. Note that this result is obtained for any finite value of σ/τ_m , so that the Maxwell relaxation time is not measurable even if $\sigma \ll \tau_m$.

Figure 3 shows the results for the single relaxation time Maxwell model, with $\tau_m/\tau_b = 10^{12}$ as found in experimental studies (see the Discussion section). Note in Fig. 3(a) that the mean-squared displacement oscillations, with period $\sim 2\pi\sqrt{\tau_b \tau_m}$, cannot be distinguished for $t > \sigma > 2\pi\sqrt{\tau_b \tau_m}$.

IV. DISCUSSION

Using a relatively simple model for the dynamic error, we can quantify the effect of the acquisition time on the mean-squared displacement of thermally fluctuating particles in a complex medium. Moreover, most of the trends of the Voigt and Maxwell models are captured with the simple power-law relaxation model.

The complex shear modulus spectrum $G^*(\omega)$ can be evaluated using the generalized Stokes-Einstein relation obtained in the inertialess limit [3,4],

$$\tilde{G}(s) = \frac{k_B T}{s \pi a \langle \Delta \tilde{\mathbf{x}}^2(s) \rangle} \text{ with } G^*(\omega) = \tilde{G}(i\omega), \quad (31)$$

where $\tilde{G}(s)$ and $\langle \Delta \tilde{\mathbf{x}}^2(s) \rangle$ are the Laplace transform of the shear modulus and of the mean-squared displacement, s being the Laplace frequency.

For the Voigt model, we can use the inertialess limit Eq. (17) for the mean-squared displacement to find

$$\overline{G^*}(\omega, \sigma) = \frac{G}{\epsilon_\sigma} \frac{1 + i\omega\tau_v}{1 + i\omega\tau_v(1 - \beta_\sigma)}. \quad (32)$$

Using the approximation given by Eq. (26) for the Maxwell model, we find

$$\overline{G^*}(\omega, \sigma) = \frac{G}{\epsilon_\sigma} \frac{i\omega\tau_m\epsilon_\sigma}{1 + i\omega\tau_m\epsilon_\sigma}. \quad (33)$$

These apparent shear modulus spectra are compared to the exact expressions Eqs. (8) and (20) in Fig. 4.

To evaluate the error ϵ_σ , one must compare the acquisition time σ to the onset time of the plateau. In the Maxwell model and the underdamped Voigt model, the ballistic regime observed before the plateau is extended to an onset time $\sqrt{\tau_b\tau_m}$ and $\sqrt{\tau_b\tau_v}$, respectively. These timescales can be understood with a simple picture. In the elastic regime, the particle moves in a harmonic well $U(x) = kx^2$, with $k = 6\pi aG$ and where G is the elastic modulus of either the Voigt or the Maxwell fluid. Since the particle equilibrium energy is $k_B T$, it moves in a range $x = \pm \sqrt{k_B T/k}$. The time required to sample this range at the equilibrium velocity $\sqrt{k_B T/m}$ is then $\sqrt{m/k}$, equal to, respectively, $\sqrt{\tau_b\tau_v}$ or $\sqrt{\tau_b\tau_m}$ in the Voigt or the Maxwell model.

This simple picture of a particle in a harmonic potential well helps to understand the effect of the sampling and the common trends observed for the apparent plateau values as σ increases. In a time interval of length τ , the particle has sampled all possible positions in the potential well. Thus, when averaged over a time interval $\sigma > \tau$, its apparent position remains constant equal to the potential center, and the apparent mean-squared displacement tends to 0.

Few microrheology experiments have been performed on single relaxation time fluid models. In a study by van Zanten and co-workers [13], measurements were performed on CTAB/KBr wormlike micelle aqueous solution using diffusing wave spectroscopy with $2a \approx 1 \mu\text{m}$ diameter polystyrene beads for probe particles. This technique provides a high temporal resolution of $\sigma \approx 10^{-6}$ s limited by the sampling

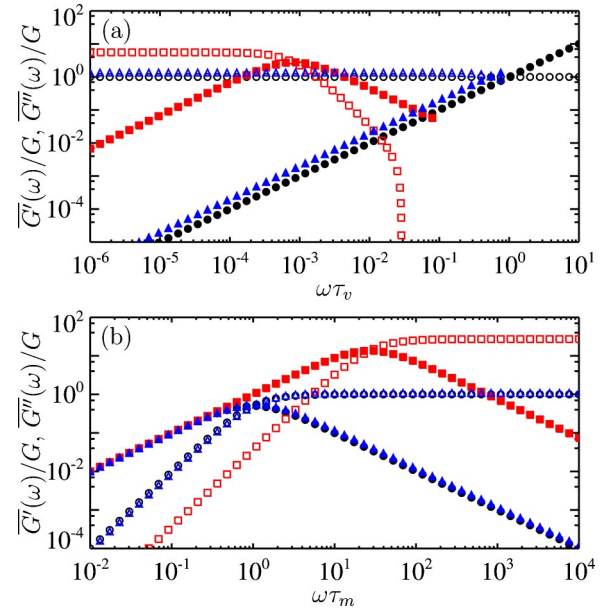


FIG. 4. (Color online) Apparent shear modulus spectrum for the Voigt model (a) and the Maxwell model (b) obtained from Eqs. (32) and (33), respectively. The open symbols show the apparent storage modulus $\overline{G'}$ (real part of $\overline{G^*}$) and the filled symbols give the loss modulus $\overline{G''}$ (imaginary part of $\overline{G^*}$). Circles are the exact values [from Eq. (8) in (a) and Eq. (20) in (b)]. The triangles and squares are the apparent values with σ being, respectively, equal to the plateau onset time [$\sigma = \tau_v$ in (a) and $\sigma = \sqrt{\tau_b\tau_m}$ in (b)] and 10 times the plateau onset time [$\sigma = 10\tau_v$ in (a) and $\sigma = 10\sqrt{\tau_b\tau_m}$ in (b)]. We took $\tau_m/\tau_b = 10^{12}$ for (b).

frequency of the multiple-tau digital correlator as used for lag times larger than $\sim 1 \mu\text{s}$ [14]. Under the conditions they used [19], both rheological and microrheological measurements show a single relaxation time Maxwellian behavior of the solution. From their data we find $\sigma/\sqrt{\tau_b\tau_m} \approx 10$ and $\tau_m/\tau_b \approx 10^{12}$. For these values, the use of Eq. (25) shows that the apparent plateau is less than 5% of the true values, which corresponds to a factor of 20 for the error in the estimated elastic modulus G (see Fig. 4). However, the plateau moduli estimated by van Zanten and co-workers are in good agreement with rheological measurement [13]. Another plateau onset time $\tau_e > \sigma$ is involved in the dynamics. They suggest that for $t < \tau_e$ the particle's dynamics is driven by the Rouse behavior of the wormlike micelles, that is, $\langle \Delta \mathbf{x}^2(t) \rangle \propto t^{1/2}$ [15]. We can modify our power-law relaxation model to take the Maxwell behavior into account by setting

$$\frac{\langle \Delta \mathbf{x}^2(t) \rangle}{\langle \Delta \mathbf{x}_p^2 \rangle} = \begin{cases} (t/\tau_e)^{1/2} & \text{if } t \leq \tau_e, \\ (t - \tau_e)/\tau_m + 1 & \text{if } t > \tau_e. \end{cases} \quad (34)$$

If we take $\tau_e/\tau_m = 10^{-3}$ and $\sigma/\tau_m = 10^{-5}$, we find that the dynamic error diminishes the plateau value by only 5%.

It is instructive to consider the dynamic error arising in the same experimental system when studied by the commonly employed technique of video microscopy [6–8]. Standard video microscopy uses an industrial grade CCD camera for signal detection with usually $\sigma \approx 10^{-3}$ s. If the experi-

mental Maxwell model fluid described here was studied with video microscopy (then $\sigma/\tau_m \approx 10^{-2}$ and $\sigma/\tau_e \approx 10$), we predict that the dynamic error will lead to a great discrepancy between the microrheology measurements and the bulk rheology (Fig. 4). This dramatic comparison reinforces the need to understand the dynamic error when performing microrheology using different setups.

V. CONCLUSION

We investigated the effect of a finite exposure time on microrheology measurements of fluids in which an embedded particle's mean-squared displacement displays a plateau

above an onset time τ . Using common viscoelastic models, we find that the sampling rate σ^{-1} has a great effect on the measured shear modulus. In particular, the latter exhibits apparent magnitudes that greatly differ from the expected value when σ is larger than τ and our calculations allow us to quantify these effects. In general, at frequencies $\omega \lesssim \sigma^{-1}$, extracted scalings and analysis should be performed with great care.

ACKNOWLEDGMENTS

The authors thank J. H. van Zanten for insightful discussions. This work was supported by the DuPont-M.I.T. Alliance.

-
- [1] F. C. MacKintosh and C. F. Schmidt, *Curr. Opin. Colloid Interface Sci.* **4**, 300 (1999).
- [2] B. Schnurr, F. Gittes, F. C. MacKintosh, and C. F. Schmidt, *Macromolecules* **30**, 7781 (1997).
- [3] T. G. Mason and D. A. Weitz, *Phys. Rev. Lett.* **74**, 1250 (1995).
- [4] T. G. Mason, *Rheol. Acta* **39**, 371 (2000).
- [5] A. J. Levine and T. C. Lubensky, *Phys. Rev. E* **63**, 041510 (2001).
- [6] M. J. Solomon and Q. Lu, *Curr. Opin. Colloid Interface Sci.* **6**, 430 (2001).
- [7] M. L. Gardel, M. T. Valentine, and D. A. Weitz, in *Microscale Diagnostic Techniques*, edited by K. Breuer (Springer-Verlag, Berlin, 2005).
- [8] T. Savin and P. S. Doyle, *Biophys. J.* **88**, 623 (2005).
- [9] M. Keller, J. Schilling, and E. Sackmann, *Rev. Sci. Instrum.* **72**, 3626 (2001).
- [10] A. Papoulis, *Probability, Random Variables, and Stochastic Processes*, 3rd ed. (McGraw-Hill, New York, 1991).
- [11] P. M. Chaikin and T. C. Lubensky, *Principles of Condensed Matter Physics* (Cambridge University Press, Cambridge, U. K., 1995).
- [12] V. S. Volkov and A. I. Leonov, *J. Chem. Phys.* **104**, 5922 (1996).
- [13] J. H. van Zanten and K. P. Rufenner, *Phys. Rev. E* **62**, 5389 (2000).
- [14] K. Schätzel, M. Drewel, and S. Stimac, *J. Mod. Opt.* **35**, 711 (1988).
- [15] M. Doi and S. F. Edwards, *The Theory of Polymer Dynamics* (Oxford University Press, Oxford, 1986).
- [16] In Fig 1(d), one cannot see $\bar{\alpha}(\sigma, \sigma) \rightarrow \alpha$ as $\sigma \rightarrow 0$. In that limit, both t and σ are tending to 0 together since we set $t = \sigma$. One can show, however, that $\bar{\alpha}(t, \sigma) = \alpha(t) + O((\sigma/t)^\nu)$ with $\nu > 0$.
- [17] Note that the plateau scaled value obtained from Eq. (24) is $1 - \tau_b/\tau_m$.
- [18] We use $1/\tau_+ + 1/\tau_- = 1/\tau_m$. Note that this approximation returns the inertialess limit for $\sigma = 0$: $\langle \Delta \bar{\mathbf{x}}^2(t, \sigma = 0) \rangle / \langle \Delta \mathbf{x}_p^2 \rangle \approx t/\tau_m + 1$.
- [19] At the concentration used ($[\text{CTAB}] \approx 0.3 \text{ M}$ and $[\text{KBr}] \approx 1 \text{ M}$) and at $T \approx 35^\circ \text{C}$, the solution is Maxwellian in the vicinity of a relaxation time $\tau_m \approx 0.1 \text{ s}$ with a high-frequency elastic plateau at $G \approx 1000 \text{ Pa}$. The Brownian time can be calculated with $\tau_b = 2a^2\rho/(9G\tau_m) \approx 10^{-13} \text{ s}$, where $\rho \approx 1000 \text{ kg/m}^3$ is the particle density.